⌯Understanding Controlling Factors of Extratropical Humidity and Clouds with an Idealized General Circulation Model

MICHELLE E. FRAZER[a,b] AND YI MING[c]

[a] *Program in Atmospheric and Oceanic Sciences, Princeton University, Princeton, New Jersey*
[b] *Department of Geosciences, The Pennsylvania State University, State College, Pennsylvania*
[c] *NOAA/Geophysical Fluid Dynamics Laboratory, Princeton, New Jersey*

ABSTRACT: This paper examines the physical controls of extratropical humidity and clouds by isolating the effects of cloud physics factors in an idealized model. The Held–Suarez dynamical core is used with the addition of passive water vapor and cloud tracers, allowing cloud processes to be explored cleanly. Separate saturation adjustment and full cloud scheme controls are used to consider the strength of advection–condensation theory. Three sets of perturbations to the cloud scheme are designed to test the model's sensitivity to the physics of condensation, sedimentation, and precipitation formation. The condensation and sedimentation perturbations isolate two key differences between the control cases. First, the sub-grid-scale relative humidity distribution assumed for the cloud macrophysics influences the location and magnitude of the extratropical cloud maxima, which interrupt the isentropic transport of moisture to the polar troposphere. Second, within the model's explicit treatment of cloud microphysics, re-evaporation of hydrometeors moistens and increases clouds in the lower troposphere. In contrast, microphysical processes of precipitation formation (specifically, the ratio of accretion to autoconversion) have negligible effects on humidity, cloudiness, and precipitation apart from the strength of the large-scale condensation and formation cycle. In addition, counterintuitive relationships—such as cloud condensate and cloud fraction responding in opposing directions—emphasize the need for careful dissection of physical mechanisms. In keeping with advection–condensation theory, circulation sets the patterns of humidity, clouds, and precipitation to first order, with factors explored herein providing secondary controls. The results substantiate the utility of such idealized modeling and highlight key cloud processes to constrain.

KEYWORDS: Cloud microphysics; Cloud parameterizations; Clouds; General circulation models; Idealized models

1. Introduction

Cloud feedback is widely considered to be the largest contributor to the intermodel spread in climate sensitivity among comprehensive general circulation models (GCMs; e.g., Ceppi et al. 2017; Sherwood et al. 2020). Bony et al. (2015) argued that consensus among most comprehensive GCMs does not, on its own, yield robust conclusions on cloud feedback. Rather, theories that underpin physical arguments and improve understanding in a way that allows for expanded use and interpretation of comprehensive GCMs are an additional requirement. Thus, simple models whose workings can be clearly grasped play a key role in the midst of a complex scientific problem (Pierrehumbert et al. 2007; Held 2005, 2014). If a GCM produces both observationally constrained cloud fields and multimodel consistent cloud feedbacks, but without the physical mechanisms necessarily being represented appropriately, its prediction of the climatic response to a radiative forcing may be significantly flawed. With the potential for unrealistic interactions between different parameterized processes (Ceppi et al. 2017), decomposition of the effects of individual processes could lead to improved parameterizations.

Here, we study underconstrained cloud macrophysical and microphysical processes by exploring the underlying physical mechanisms. Since changing a stratiform cloud scheme can have significant ramifications, even reversing a model's feedback with warming (Geoffroy et al. 2017), we use an idealized setup to break down a cloud scheme and understand the effects of individual cloud processes on atmospheric humidity and cloudiness. The processes studied herein are motivated by three factors: understanding the differences between the advection–condensation theory of humidity and a cloud scheme, the controls of large-scale precipitation efficiency, and the direct effect of stratiform-cloud related GCM parameters on free tropospheric humidity and clouds.

a. Advection–condensation theory

Free tropospheric humidity is important to the distribution of clouds and precipitation. The so-called advection–condensation theory suggests that water vapor (WV) in the atmosphere is most simply reflective of the lowest temperature (lowest saturation specific humidity) experienced by the parcel since leaving the nearly saturated surface layer. This theory alone can describe WV distribution to first order (Sherwood et al. 2010). Advection–condensation theory helps explain two key features of free tropospheric humidity: dry subtropical zones and moist polar regions connected by dry isentropes.

Pierrehumbert (1998) laid out three factors that contribute to the dry subtropics. First, subsidence brings down dry air, and would keep the region at the mixing ratio of the tropopause

if not for other mechanisms. Second, lateral mixing brings in moist air from the tropical convective region. Third, processing of air through cold extratropics dries the region. Thus, the dry subtropics and moist poles are connected through nearly isentropic large-scale advection, and cycling through cold polar upper-tropospheric air is a key means of dehydrating air in the extratropics (Kelly et al. 1991). Pierrehumbert (1998) also noted the role of re-evaporation of hydrometeors as a subtropical moisture source as emphasized by Sun and Lindzen (1993) but suggested that this is limited by weak rainfall. Also suggesting the importance of in situ moistening processes in the midlatitudes, Yang and Pierrehumbert (1994) showed that in the advection–condensation model, the tropical moisture source is too inefficient (i.e., too weak of mixing between tropics and extratropics). These factors have been expounded in further work.

Using a simple saturation adjustment scheme as a representation of advection–condensation theory, Galewsky et al. (2005) found that the primary dynamical control of the dry subtropics was isentropic dehydration by midlatitude eddies (with diabatic descent through Hadley circulation playing a secondary role). WV is transported from the lower deep tropics to the upper polar extratropics by baroclinic eddies along isentropes, with the moist air rising and cooling adiabatically. The storm tracks interrupt the transport such that significant moisture is released through precipitation before reaching the poles. Thus, the return flow supplies dehydrated air to the subtropics, and is confined to isentropic layers (Held and Schneider 1999). The poleward eddy WV transport follows dry isentropes but different values of equivalent potential temperature, with this moist recirculation peaking on the equatorward side of the storm tracks (Laliberté et al. 2012). In this study, we consider how a cloud scheme distributes moisture differently than simple saturation adjustment [as in Galewsky et al. (2005)], and we highlight the processes—cloud macrophysics and microphysics alike—that affect extratropical humidity strongly. The physical mechanisms of these controls are delineated to highlight those processes that need to be represented accurately in cloud schemes.

b. Precipitation efficiency controls

Differences between saturation adjustment and a cloud scheme are closely related to the controls of precipitation efficiency. The residence time of water in the atmosphere is, in a full cloud scheme, affected by three efficiencies: the efficiency with which WV may become cloud condensate (condensation), become part of a falling hydrometeor (formation), and reach the surface as precipitation (sedimentation) (Langhans et al. 2015). Advection–condensation theory reduces this complexity to one efficiency since WV in excess of saturation immediately becomes surface precipitation. Thus, condensation and sedimentation efficiencies highlight two of the key differences between a saturation adjustment scheme (based on advection–condensation theory) and a full cloud scheme (closer to reality): condensation efficiency is affected by assumptions of small (subgrid) scale relative humidity (RH) distribution, and sedimentation efficiency by re-evaporation of precipitation. The third efficiency—formation efficiency—can be affected by internal

cloud scheme parameters such as the assumed cloud condensation nuclei (which affects warm rain processes) or the fall speed of ice. But each of the three efficiencies have the potential to significantly affect WV and cloud condensate (CC) fields, the distribution of precipitation, and the overall residence time of atmospheric water. For example, precipitation efficiency (the multiplicative product of formation and sedimentation efficiencies; see section 2b) is frequently highlighted as being potentially affected by warmer temperatures resulting in more liquid at the expense of ice in mixed-phase clouds (Klein et al. 2009; McCoy et al. 2015; Ceppi et al. 2016; McCoy et al. 2018). Here we explore the direct effect of changing these efficiencies on steady-state fields that are relevant to radiative feedbacks.

c. GCM stratiform tuning parameters

Thus, the first two motivations are connected to the third of the direct effect of stratiform-cloud-related GCM tuning parameters on free tropospheric humidity and clouds. Critical RH (the minimum GCM gridbox-mean RH needed for cloud condensate formation) is a useful tuning parameter for radiative balance (through shortwave cloud radiative effects) but may be tuned artificially high to compensate for too-bright clouds (McCoy et al. 2016). Critical RH is important because it controls large-scale condensation, a sink of WV and source of CC. WV can be altered without directly affecting CC by tuning the re-evaporation of precipitation. Another key parameter is the assumed cloud drop number concentration N: aerosols affect microphysics and thus precipitation and radiation through aerosol–cloud interactions. The observed precipitation rate can be expressed as a power-law function of liquid water path (LWP) and N, with a strong correlation between LWP and the ratio of accretion to autoconversion processes (hereinafter accr/auto; Jiang et al. 2010). At low LWP, accr/auto is small because of few generated raindrops. Some GCMs directly model aerosol indirect effects, but even in simpler cloud microphysics schemes that lack an explicit representation of aerosol indirect effects, the autoconversion process is a direct function of N and thus a major control of accr/auto, which is a key parameter for examining the balance of microphysical conversion processes from cloud water to rainwater (e.g., Gettelman et al. 2013).

In a GCM study implementing five different autoconversion schemes, Michibata and Takemura (2015) found significant variance in accr/auto. However, these schemes showed a commonality of the relative role of the accretion process being underestimated by one or more orders of magnitude relative to observations [as estimated by Gettelman et al. (2013)]. This incorrect ratio comes from both too high simulated autoconversion rates (Gettelman et al. 2013, 2014) and in some schemes, too low of an accretion enhancement factor for correct precipitation intensity (Wu et al. 2018). The high simulated autoconversion rates come from diagnostic precipitation that forms warm rain too easily (Jing et al. 2017). Cloud condensation nuclei and accr/auto affect not only precipitation rates but also radiative forcing. Increased accr/auto in GCM

simulations is correlated with increasing LWP (Gettelman et al. 2013), and cloud optical depth and thus shortwave radiative effect is significantly controlled by LWP (e.g., Stephens 1978). As past studies have likely underestimated the true sensitivity of clouds and radiation to aerosols, the negative forcing of the Twomey effect (altered cloud albedo from increased anthropogenic aerosols) may be underestimated (Quaas et al. 2020), although the aerosol–cloud lifetime effect may be overestimated (e.g., Quaas et al. 2009). Yet, Gettelman et al. (2013) suggested that the autoconversion rate bias can be corrected by altering the relative balance of the autoconversion and accretion rates, which lowers the radiative effect of aerosol cloud interactions. Thus, understanding the interplay and impacts of altered N and accr/auto is critical.

d. Purpose and organization

The overarching purpose of this paper is to employ an idealized model setup to shed light on what controls free tropospheric humidity and cloudiness. Using perturbation experiments that isolate key processes, we aim at elucidating the complex connections among WV, clouds, precipitation, and circulation. In analyzing the control and perturbation experiments in this study, the budgetary terms of the cloud scheme that represent the conversions among WV, CC, and precipitating water P are particularly emphasized. This method is motivated by a need for a robust physical understanding to ground model representations of cloud processes so as to lend confidence to model-inferred relationships (Shepherd 2014; Stevens and Bony 2013).

A process-based analysis is related to the secondary purpose of this work: to clearly demonstrate the value of this modeling tool (a dry GCM with passive water and cloud tracers) for developing a systematic understanding of physical controls on humidity and clouds and diagnosing their representations in models. This approach is in the same spirit as "mechanism-affirmation experiments" described in Jeevanjee et al. (2017) as being the provision of a model hierarchy framework. In terms of the model hierarchy, the setup used in this paper (Ming and Held 2018) is derived from the Held–Suarez (HS; Held and Suarez 1994) dry GCM, but in a different direction than the Frierson moist aquaplanet GCM (Frierson et al. 2006), which extended the HS dry GCM by adding a gray radiation scheme and moist physics such that latent heating affects the model's dynamics. Our model is in many aspects more idealized than the Frierson model with dry dynamics and no radiation scheme, but more complex in its addition of a full cloud microphysics scheme. It can be thought of as one rung higher on the model hierarchy ladder than the HS dry GCM, but one rung lower than the Frierson model. This setup is therefore uniquely suitable for answering specific questions about extratropical humidity and cloudiness—namely the direct effects of cloud macrophysics and microphysics—as well as the physical mechanisms behind these effects. With passive humidity and cloud tracers, isolated experiments are able to be performed such that the direct effect of a cloud physics process can be clearly diagnosed without the convoluting circular effects of dynamical processes.

This paper is organized as follows. Section 2 lays out the method of this study, describing the idealized model, experiments, and analysis framework. Section 3 describes the results from the control saturation adjustment and cloud physics experiments and the condensation, sedimentation, and formation perturbations. Section 4 discusses the implications of these results for the value of the advection–condensation paradigm, key stratiform cloud physics processes to constrain, and the utility of this idealized model.

2. Method

a. Control models

The idealized model used here is based on the HS dry GCM (Held and Suarez 1994) with the addition of four passive water and cloud tracers—specific humidity, cloud liquid, cloud ice, and cloud fraction (CF)—as described in Ming and Held (2018). The dry GCM uses a hydrostatic spectral dynamical core for an ideal gas atmosphere with no topography. For this work, a resolution of T42 (referring to the maximum number of zonal waves present in the triangular truncation) is used, resulting in a horizontal grid of 128 by 64 cells (about 2.8° spacing) with 20 vertical layers equally spaced in the sigma coordinate. The forcing consists of Newtonian relaxation of temperature toward a prescribed zonally symmetric equilibrium temperature and planetary boundary layer drag represented by Rayleigh damping. This idealized setup enables the isolation of the roles of various cloud processes. It assumes that latent heating or cooling from conversions among WV, CC, and precipitation do not feed back on the dynamics. Also, with no explicit radiation scheme in the model, clouds do not affect circulation through cloud radiative effects. Thus, WV and clouds are passive in that they do not affect circulation or temperature patterns.

Two control simulations are created with results explored in section 3a. The first, referred to as the *Base* case, uses only the specific humidity tracer in a saturation adjustment scheme modeled after Galewsky et al. (2005) as a direct representation of advection–condensation theory. Any water in excess of saturation (gridbox mean) is assumed to fall out immediately as precipitation. Thus, no clouds are present. The second control simulation is referred to as the *Cloud* case. It carries specific humidity, cloud liquid, cloud ice, and CF tracers through the same large-scale cloud macrophysics scheme as implemented in the GFDL HiRAM model (Zhao et al. 2009). The cloud scheme assumes a beta distribution for sub-grid-scale total water (which includes both WV and CC). CF is diagnosed from this total water-based RH, which varies only slightly from traditional RH (which is based on WV only and is the RH reported in the results). The default beta distribution is such that a grid-mean total water-based RH value exceeding 83.3% (the critical RH: RH_c) allows for subgrid values greater than 100% and thus a nonzero CF for the grid box.

The pathways for conversion between WV, cloud liquid, cloud ice, and hydrometeors follow a Rotstayn-Klein single-moment microphysics scheme (Rotstayn 1997; Rotstayn et al. 2000). Additionally, as the principal source of WV, surface

evaporation is represented by adjusting the specific humidity of grid boxes below ~850 hPa toward saturation with an *e*-folding time scale of 30 min. Microphysical sources of WV are large-scale (LS) evaporation of cloud liquid, LS sublimation of cloud ice, rain evaporation, and snow sublimation. The only sinks of WV—LS condensation and LS deposition—are also the only sources of CC. CC is lost to WV through LS evaporation and LS sublimation, to rain through autoconversion, accretion, and melting of cloud ice, and to snow through gravitational settling. Additionally, cloud liquid is converted to cloud ice through riming, the Bergeron–Findeisen process, and homogeneous freezing, and both cloud ice and snow can be converted to rain through melting. (Cloud ice and snow have identical properties such as fall speed and are simply distinguished by their location in or out of a cloud.) See Fig. 1 in Frazer and Ming (2022) and the descriptive text for more details of these conversions.

b. Perturbation experiments

On the surface, there are three chief distinctions between saturation adjustment (Base control) and a full cloud scheme (Cloud control). First, clouds can form (and thus precipitation is possible) before the grid box is fully saturated through RH_c and an assumed sub-grid-scale RH distribution. Second, the cloud scheme allows precipitation to evaporate before reaching the surface through rain evaporation and snow sublimation (RESS). Third, cloud condensate may be advected before precipitating out or evaporating. The effects of the first two distinctions can be easily explored by being simply "turned off" in the cloud scheme. The third is inferred as a residual effect.

Each of the three distinctions correspond to the three efficiencies that affect the residence time of water in the atmosphere and form a key part of the analysis. We make use of the explicit/large-scale precipitation efficiency (PE) as defined in Zhao (2014) to represent the total PE, since only stratiform (not convective) precipitation is represented in this model. PE is the ratio of surface precipitation to vertically integrated CC sources, and thus represents the fraction of condensed particles that subsequently rain out. Following Langhans et al. (2015), PE can be thought of as the product of formation efficiency (FE) and sedimentation efficiency (SE): PE = FE × SE; FE represents the probability of formation given condensation, and SE represents the probability of sedimentation given formation. The condensation efficiency (CE) is used herein to simply represent the fraction of atmospheric WV that subsequently condenses (as there is no explicit treat of entrainment in this stratiform scheme). Thus, CE is the ratio of CC sources (condensation and deposition) to WV sources (surface evaporation, CC evaporation and sublimation, and RESS), FE is the ratio of precipitation formation (autoconversion, accretion, melting of cloud ice, and gravitational settling) to CC sources, and SE is the ratio of surface precipitation to precipitation formation. Additionally, the residence (or recycling) time for WV in the atmosphere is defined, following Trenberth (1998), as the *e*-folding time constant for the depletion of precipitable water by precipitation (i.e., the global ratio of column-integrated WV to the precipitation rate). These indicators of features of the water cycle are used to quantify changes in the WV, CC, and precipitation budgetary

terms to supplement the analysis of steady-state fields. Also, because these efficiencies correspond to distinctions between saturation adjustment and a cloud scheme, we intentionally alter the efficiencies to understand the effects on steady-state fields. CE is affected by RH_c, SE is 100% without RESS, and FE cannot be defined without CC.

Thus, three principal perturbation experiments are designed, testing sensitivity to condensation, sedimentation, and formation cloud processes. The condensation perturbation focuses on the conversion between WV and CC through cloud macrophysics, specifically sub-grid-scale cloudiness. The first key distinction between saturation adjustment and a cloud scheme can be eliminated by removing sub-grid-scale cloudiness and requiring 100% grid-mean RH for cloud formation. Accordingly, an intermediate setup between the Base and Cloud controls is created by reducing the width parameter of the beta distribution defining sub-grid-scale RH from 0.2 to 0.01, effectively requiring 100% gridbox-mean RH for cloud formation. This perturbation run is referred to as *RHc100* (since effectively $RH_c = 100\%$) with results in section 3b.

The sedimentation perturbation focuses on the role of re-evaporation of hydrometeors. While saturation adjustment oversimplifies the variety of conversions in this Rotstayn-Klein microphysics scheme, it is analogous to the LS phase changes and precipitation processes. The chief remaining processes are the recycling of hydrometeors back to WV through RESS. Thus, another intermediate setup between the controls is created to illuminate the significance of RESS. For this experiment—*noRESS*, which is presented in section 3c—the rates of RESS are arbitrarily set to zero. In addition, to examine the combined effect of the key microphysical and macrophysical differences between the Base and Cloud cases, a final intermediate case is considered. The *RHc100_noRESS* case includes $RH_c = 100\%$ and omission of RESS effects to examine residual differences between the control cases, which is assumed to correspond to the third key difference between saturation adjustment and full cloud physics—advection of CC—as explored in section 4.

The formation perturbation is not focused directly on a difference between the Base and Cloud cases. In the Base case saturation adjustment, precipitation is formed directly from WV in a manner more similar to condensation than formation. Rather, formation is explored so that sensitivity to all key conversions of the cloud scheme is considered. Formation consists of three major processes: autoconversion, accretion, and ice settling. Ice settling is a net term—the difference between ice falling into and out of grid boxes. Accordingly, autoconversion and accretion were isolated as the best processes to perturb so as to explore formation sensitivities. From a general perspective, if autoconversion or accretion is arbitrarily reduced in this model, the other process strengthens to keep formation close to constant, but somewhat reduced. Conversely, if one process is amplified, the other weakens. An analogous effect results from altering the prescribed cloud drop number concentration, N, the default value being 50 cm^{-3}. For autoconversion to occur, the radius of the cloud droplets—a function of N—must be greater than the critical particle radius threshold at which autoconversion occurs, and autoconversion increases directly with increasing

TABLE 1. Description of the experiments.

Name	Description
Base	Control simulation with specific humidity tracer and saturation adjustment
Cloud	Control simulation with specific humidity and cloud tracers (liquid, ice, and fraction) and microphysics
RHc100	Variant of Cloud simulation requiring 100% gridbox-mean RH for cloud formation (RH_c)
noRESS	Variant of Cloud simulation without rain evaporation or snow sublimation
halvAUTO	Variant of Cloud simulation halving the raw computed value for autoconversion at each time step
doubAUTO	As halvAUTO, but doubling autoconversion
RHc100_noRESS	Variant of Cloud simulation combining both RHc100 and noRESS variations

N. Increased autoconversion should have two effects on accretion: increasing the flux of rain (to scavenge cloud liquid) and decreasing the pool of cloud liquid available to be scavenged. Here, the second effect wins out such that if N is decreased, autoconversion increases and accretion decreases with a net amplification of formation. An increase of N produces an opposite effect. Thus, the strength of formation and the balance between autoconversion and accretion have broader significance because of their connection to drop number concentration parameterizations.

Here, alterations to autoconversion are used to adjust accr/ auto (and indirectly explore a key affect of altered N). The principal formation perturbation explored in section 3d, *halvAUTO*, consists of halving the computed value for autoconversion for each grid box at each time step. For robustness, a corresponding doubling of autoconversion, *doubAUTO* is also examined. Note that the halving or doubling of autoconversion is performed in the microphysical code before the enforcement of a limiter, which ensures that autoconversion is limited to the amount that reduces local liquid cloud condensate to the critical value at which autoconversion begins [after Rotstayn (1997)].

For all control and perturbation experiments, the atmospheric state of the model (winds, temperature, etc.) is identical at every time step. The various experiments performed are summarized in Table 1. All model runs in this study include a 300-day spinup of the dry GCM before the next 1000 days are averaged. For figures and analysis, data are averaged between the two hemispheres because of the hemispheric symmetry of the simulated climate. The range from 15° to 90° is considered to be the subtropics and extratropics (STET) and is the focus of the analysis because of the lack of a convection scheme making the tropics nearly saturated (see Ming and Held 2018).

3. Results

a. Controls: Base and Cloud

A budgetary comparison of the control cases is shown in Fig. 1a, which depicts the principal WV tendency terms for the Base and Cloud cases from a column-integrated, zonally averaged perspective. For the Base case, the WV balance is simply between precipitation from saturation adjustment and surface evaporation. Outside of the tropics (which are not shown), the immediate precipitation dominates in the midlatitude storm tracks while evaporation occurs mostly in the subtropics, implying significant horizontal advection of water from the subtropics
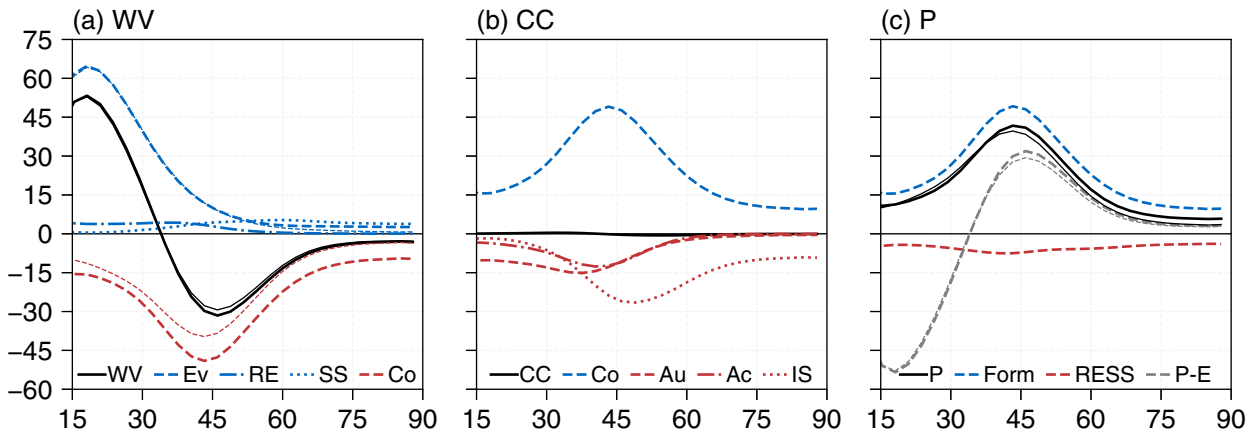

FIG. 1. Comparison of zonally averaged, column-integrated (10^{-6} kg m^{-2} s^{-1}) (a) WV, (b) CC, and (c) precipitation (P) tendency terms in control cases (black totals, blue sources, and red sinks). Cloud-case terms (depicted as indicated by the legends) shown are total water vapor (WV), surface evaporation (Ev), rain evaporation (RE), snow sublimation (SS), and net condensation (Co) in (a); total cloud condensate (CC), net condensation (Co), autoconversion (Au), accretion (Ac), and ice settling (IS) in (b); and total precipitation (P), net formation (Form), net sinks (RESS), and moisture convergence ($P - E$, i.e., surface precipitation minus evaporation) in (c). Base-case terms (depicted as half-width lines and sometimes obscured beneath their Cloud-case counterparts) shown are total WV, surface evaporation, saturation adjustment as net condensation in (a) and precipitation in (c), and saturation adjustment minus evaporation as $P - E$ in (c). A positive tendency value denotes that WV [in (a)], CC [in (b)], or precipitation [in (c)] is increasing. Totals include the less significant tendency terms that are not shown individually.

TABLE 2. Summary of STET (15°–90°) precipitation variables: average surface precipitation (P) and surface evaporation (E); condensation (CE), formation (FE), sedimentation (SE), and precipitation (PE) efficiencies; and residence time (RT). See the text for the definitions of these variables.

Run	P (mm day^{-1})	E (mm day^{-1})	CE (%)	FE (%)	SE (%)	PE (%)	RT (days)
Base	1.84	2.34	78.5	—	—	—	13.1
Cloud	1.91	2.37	83.9	98.2	79.7	78.3	12.7
RHc100	1.71	2.17	81.2	95.2	89.4	85.1	14.3
noRESS	2.00	2.47	81.3	97.9	100.0	97.9	11.8
halvAUTO	1.84	2.31	83.6	97.6	79.8	77.9	13.1
doubAUTO	1.98	2.44	84.3	98.6	79.6	78.5	12.2

(including that facilitated by midlatitude baroclinic eddies). For the Cloud case, the dominant balance between net LS condensation (condensation and deposition minus evaporation and sublimation with condensation dominating) as the main WV sink and surface evaporation as the main WV source is similar to the Base case, though RESS do make a nonnegligible contribution. Cloud case LS condensation is everywhere stronger than Base case saturation adjustment, while the surface evaporation is nearly indistinguishable except in the high latitudes where Base surface evaporation is negligible. [Surface evaporation is a direct function of low-level RH, which is similar between the Base and Cloud cases other than in the high latitudes, as discussed below. In the high latitudes, the Base case has higher RH (near saturation) and therefore minimal surface evaporation.] Thus, RESS together provide an additional source of WV, strengthening the WV cycle as opposed to replacing surface evaporation as a source. Figure 1b shows the CC budget applicable only to the Cloud case. Net LS condensation as the source of CC is balanced nearly perfectly latitudinally, implying minimal advection of CC. In the subtropics, autoconversion is the strongest sink of CC, but ice settling (snow) dominates poleward of 40° with rain processes becoming negligible poleward of 60°.

Whereas precipitation is simply saturation adjustment in the Base case but formation processes minus RESS in the Cloud case, both precipitation and precipitation minus evaporation ($P - E$) have similar latitudinal distributions in the two cases (Fig. 1c). The principal latitudinal difference is a slight increase in precipitation (and thus $P - E$) in the extratropics in the Cloud case, where ice settling (a process vastly different than saturation adjustment) dominates as the principal source of precipitation and where surface evaporation is weaker in the Base case as discussed previously. Thus, the strength of the hydrological cycle in terms of surface precipitation is largely indistinguishable with a STET average of 1.84 mm day^{-1} in the Base case and 1.91 mm day^{-1} in the Cloud case (see Table 2). This correspondence between these idealized saturation adjustment and full cloud microphysics models without any control by radiative balance suggests a significant control of the hydrological cycle by large-scale circulation perhaps mediated through RH (as discussed below).

In contrast, the strength of the WV cycle differs greatly between the two control cases. This can be seen in Figs. 2a and 2b, which depict the STET-averaged, column-integrated values and fractions of the sources and sinks in the Base and Cloud cases. The total STET WV sources and sinks in the Cloud case are 3.36×10^{-5} and 2.82×10^{-5} kg m^{-2} s^{-1},

respectively, with the regional imbalance implying advection of WV into the tropics (since evaporation is strongest in the subtropics). For comparison, the Base case analogs of surface evaporation (the only WV source) and condensation (the only WV sink) are 2.70×10^{-5} and 2.11×10^{-5} kg m^{-2} s^{-1}, respectively. Thus, the strength of the cycling of WV is significantly enhanced in the Cloud model by ~30%. Adding more sources and sinks of WV, in particular introducing sources above the boundary layer through RESS, allows for a strengthening of the WV cycle and a slight shortening of the residence time (from 13.1 to 12.7 days). In the Cloud case, CC is also cycled where all the WV sinks are CC sources, and precipitation processes are the main CC sinks (see Fig. 2b) with CC sources and sinks balanced in the STET region.

This overall picture of water cycling between WV, CC, precipitation, and an assumed surface reservoir can be seen in Fig. 3 and described in terms of efficiencies. For the STET WV produced through surface evaporation, RESS, and evaporation (LS evaporation and sublimation), 83.9% is condensed (through LS condensation and deposition). Of the water condensed, most forms precipitation, while some is evaporated (a very small effect in this model with only a stratiform cloud scheme), resulting in a FE of 98.2%. (Some also persists as condensate, but this effect is lost with time averaging.) Of the precipitation formed, ~20% is returned to WV through RESS before reaching the surface resulting in a SE of 79.7% and a PE of 78.3%. These efficiencies, along with precipitation and residence times, are summarized in Table 2. The positive WV reservoir and negative surface reservoir values are again indicative of moisture export (negative $P - E$) from the STET region.

Figure 3 also shows how a cloud scheme builds on saturation adjustment. In the Base case, only two reservoirs—WV and surface evaporation—would exist, with two arrows between them representing surface evaporation and saturation adjustment. Yet, qualitative similarity exists in the RH distribution of the Base and Cloud cases as shown in Fig. 4a. Both cases have qualitatively realistic free tropospheric RH features: the subtropics and upper troposphere are relatively dry, while the extratropics are moist (Fig. 4a). As noted in Ming and Held (2018), the high RH values in the deep tropics (not shown) and boundary layer (below 850 hPa) are due to the lack of a moist convection scheme and the way in which surface evaporation is modeled, respectively. Figure 4a suggests that the addition of a cloud scheme has two main effects on the RH distribution, while keeping the main features present.
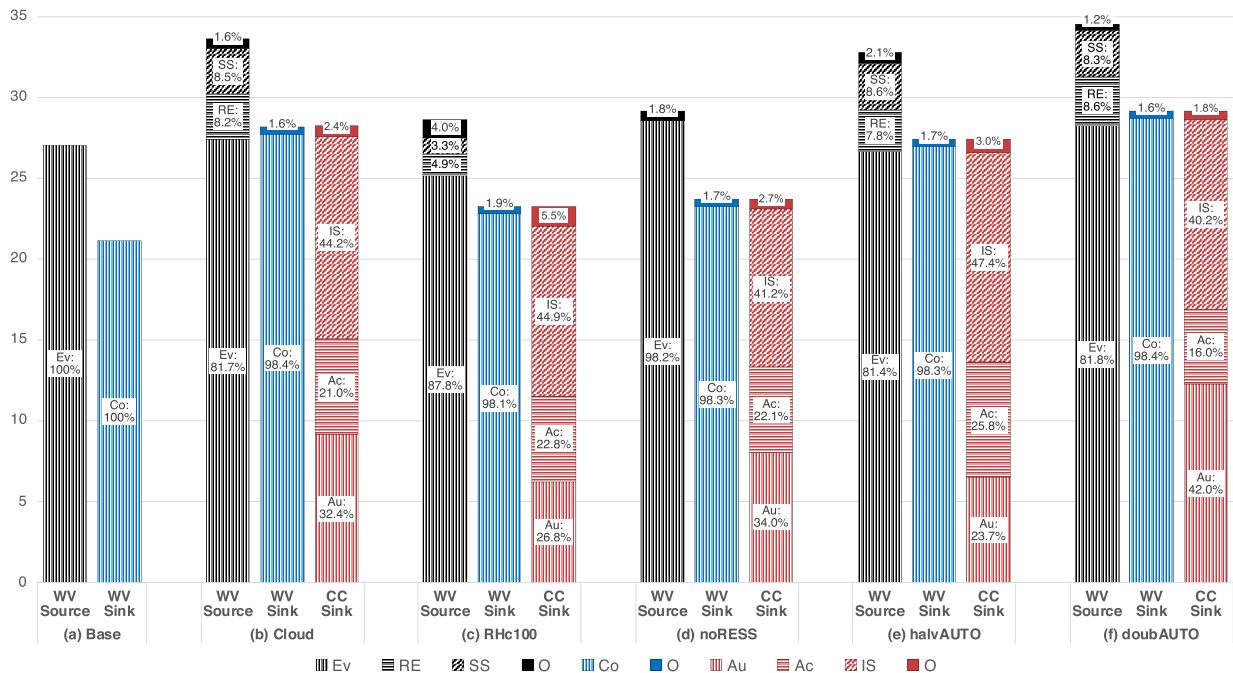
FIG. 2. Principal WV and CC sources and sinks for various model runs (see Table 1) represented as column-integrated average STET (15°–90°) tendency values (10^{-6} kg m^{-2} s^{-1}). For clarity, the smallest terms are conglomerated in an "other" (O) category. Processes shown are WV sources: surface evaporation (Ev), rain evaporation (RE), and snow sublimation (SS); WV sink (CC source): LS condensation (Co); CC sinks: autoconversion (Au), accretion (Ac), and ice settling (IS). Base-case saturation adjustment is labeled LS condensation. Percentages are given with respect to total source or sink category and may not add to 100% because of rounding.

The subtropical dry zones and nearby midlatitudes are substantially moistened with a peak increase of up to around 5% RH, while much of the polar upper troposphere becomes drier by a similar magnitude. The mechanisms for these changes are investigated in the condensation and sedimentation perturbations. Figure 4b shows the model isentropes, significant because of the established isentropic transport of moisture from the subtropics as discussed in the introduction. Here, it is clear that the polar upper troposphere (drier in the Cloud case) is connected to the subtropical boundary layer via isentropes. Yet, the overall similarity between the control cases in the free troposphere implies that RH is controlled to first order by general circulation, as opposed to cloud processes. Thus, in keeping with advection–condensation theory, one does not need detailed cloud information for understanding large-scale (first order) RH patterns.

The cloud fields generated in the Cloud case are shown in Figs. 4c and 4d. Free tropospheric CF values peak at near 30% in the extratropical storm track region, coincident with the 75% average RH contour. Liquid cloud condensate (LCC) is concentrated in the boundary layer (unrealistically high because of high RH from artificial surface evaporation as discussed above) with a secondary peak near the storm tracks. Ice cloud condensate is concentrated in a broad region near the storm tracks restricted to freezing temperatures (see Fig. 4b). Liquid cloud condensate, with its higher magnitude, dominates the spatial pattern of total CC, which is the sum of ice and liquid water

mixing ratios. Since the focus of this study is on total clouds, not on the distribution of ice versus liquid, the remainder of this work will consider only total CC, which is concentrated in the tropics with a secondary peak in the storm tracks.

b. Condensation perturbation: RHc100

As discussed in the introduction, since isentropic transport is the key source of WV for the polar regions, cloud formation (and precipitation) in the extratropical storm tracks interrupts WV reaching the polar regions. In the Cloud case, cloud formation (required for precipitation) takes place when grid-mean RH (as defined by total water) exceeds 83.3%. Therefore, one might expect a correlation between the model's extratropical cloud maxima (storm tracks) in the model and 83.3% RH contours. But cloud formation is based on instantaneous RH, not the long-term averages shown in Fig. 4c where the storm tracks are roughly collocated with the 75% RH contours. Higher RH values may occur equatorward of a given RH contour. Allowing for time variability in RH renews the possibility of a connection between the location of the storm tracks and RH distribution because of RH$_c$. This possible connection is explored with the RHc100 run, where the cloud scheme is adjusted to require essentially 100% grid-mean RH for cloud formation.

In the RHc100 case, the entire WV/CC cycle slows down significantly relative to the Cloud case (see Figs. 2b,c). Since clouds are now unlikely to form and remove moisture from the atmosphere below 850 hPa (where the air is generally nearly, but not
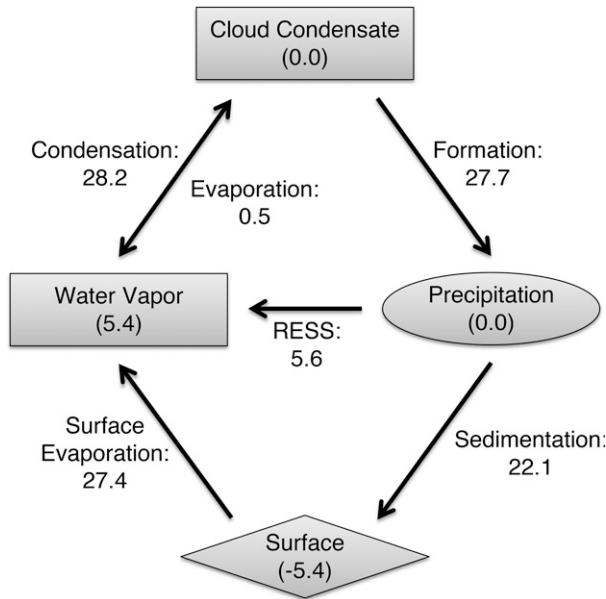
FIG. 3. Diagram of the water cycle in the control cloud microphysics scheme (Cloud experiment). Water is cycled between four species (reservoirs): WV, CC, precipitation, and an assumed surface reservoir. The quantities shown are average STET (15°–90°) tendency values (10^{-6} kg m^{-2} s^{-1}). Each reservoir shows either a balance (0.0) or an imbalance. Here, condensation comprises both LS condensation and deposition; evaporation comprises both LS evaporation and sublimation; formation includes autoconversion, accretion, ice settling, and melting of cloud ice to rain; and sedimentation represents formation processes minus RESS.

quite, saturated), surface evaporation decreases (Fig. 5a). RESS play less of a role as WV sources, approximately one-half of both the magnitude and percentage as in the Cloud case and become nearly nonexistent in the extratropics. LS condensation decreases

as a WV sink and CC source; the slowdown increases the WV residence time by 1.6 days or 13% (Table 2). This slowdown ultimately leads to a general increase in steady-state RH (Fig. 5d) for reasons discussed at length with the formation perturbation in section 3d.

The CE decreases only slightly (3%) despite the intense perturbation in condensation; CE is not a measure of how fast WV condenses, but simply whether it eventually does (in the given region, which here is the STET region). Similarly, FE decreases by 3% with a greater weakening of formation processes than condensation (see Fig. 5b). FE represents the likelihood that a water molecule, once it condenses, forms precipitation. Here, FE decreases since LS evaporation and sublimation have increased both in value and as a percentage of LS condensation/deposition. In the RHc100 setup, once a cloud is formed, if it persists to another time step where RH has decreased (as from precipitation), the remaining cloud condensate must entirely re-evaporate/sublimate. In contrast, in the Cloud case, only enough cloud condensate to match the RH-based PDF must evaporate, as long as gridbox-mean RH is above 83.3%.

The most significant change in efficiencies is SE, which increases from 79.7% to 89.4%, resulting in an amplification in PE (=FE × SE) from 78.3% to 85.1%. SE increases because of the drastic decrease in RESS from both decreased precipitation formation (Fig. 5c) as well as increased steady-state RH (Fig. 5d). While RH increases everywhere, RH is most significantly increased in regions where cloud formation at less than 100% RH had reduced the amount of WV being transported. Once a moist parcel (traveling largely poleward/upward) reaches a cold enough temperature such that the required RH is reached, excess water vapor is condensed. Thus, with 100% RH required for condensation, more WV is isentropically transported to the polar upper troposphere (and other cold regions of high RH) before clouds are formed. Weakened RESS results from less precipitation falling through moister air, especially in the extratropics
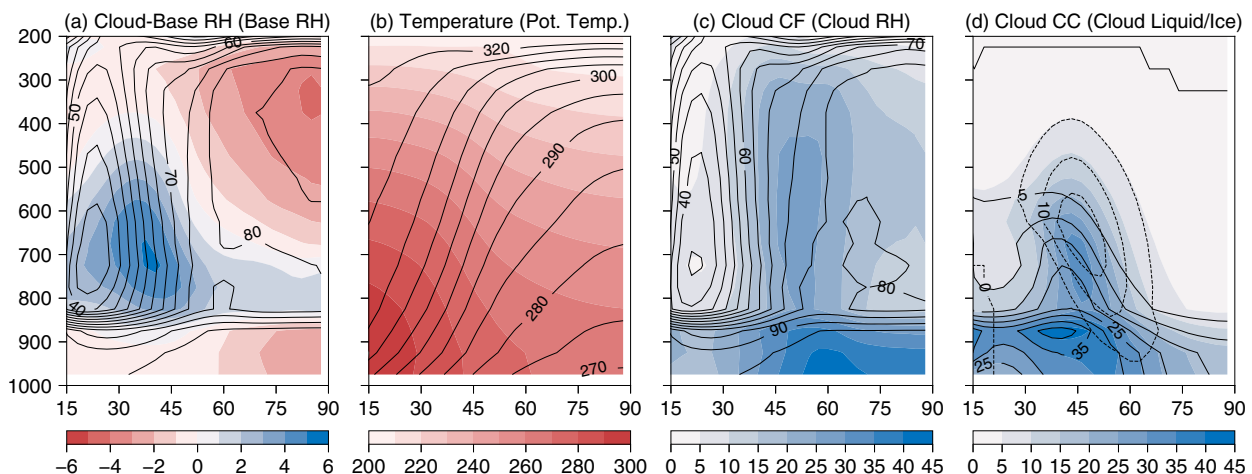

FIG. 4. Key variables in control runs: (a) RH difference (Cloud minus Base; %) as shading and Base RH as contours (5% spacing), (b) temperature (K) as shading and potential temperature as contours (5-K spacing), (c) Cloud CF (%) as shading and Cloud RH as contours (5% spacing), and (d) Cloud total CC (10^{-6} kg kg^{-1}) as shading and liquid (solid) and ice (dashed) CC as contours (5×10^{-6} kg kg^{-1} spacing). Variables have been zonally averaged, and the x and y axes are latitude and pressure (hPa), respectively.

where the increase in RH is most significant. Ultimately, despite increased PE, there is a 10% reduction in STET surface precipitation (Table 2) potentially driven by decreased CC in the boundary layer (discussed below).

In addition to an increase in RH, with the RHc100 setup, CF is significantly amplified in the polar extratropics (Fig. 5e). With seemingly more difficult conditions for cloud formation, CF increases everywhere (above 850 hPa). This can be understood by considering what triggers cloud formation in the cloud scheme: high values of RH. The increase in average RH noted previously does in fact correspond to a rise in occurrences of high RH as shown through a histogram of daily RH values (Fig. 5g) where values in the [100%, 105%] bin increase drastically but all other values decrease slightly. A histogram of daily CF values (Fig. 5h) shows a decrease in CF values below 65% and a drastic rise in occurrences of the highest values with the final bin being the highest populated. (Note that while RH values greater than 100% are possible, by definition, 100% is the maximum possible CF value such that the final CF histogram bin represents values of exactly 100% CF.) With 100% grid-mean RH required for cloud formation, when cloud formation is triggered it must be 100% CF at the time step of the model. These histograms were further broken down by meridional and vertical flow directions (not shown). Poleward and upward flows accounted for the highest RH values and thus the higher CF values, but overall the stratified histograms painted the same picture. For every direction of flow, the RHc100 perturbation requires greater RH for cloud formation, increasing high RH values and thus CF. Accordingly, the location of maximum storm track cloudiness shifts poleward (to areas of greater RH) from ~50° (Fig. 4c) to ~60° (not shown).

While CF increases significantly, the change in CC in the free troposphere is small, and in most places is a decrease as seen in Fig. 5f. (A significant loss of CC below 850 hPa not shown is a result of the region being generally unsaturated, since surface evaporation is associated with a time scale.) While changes in CF and CC need not totally align, such drastic differences are surprising and are, in fact, largely an artifact of altering the macrophysics in a way that is unexpected by the microphysics scheme. With the RHc100 condition, if clouds form in a grid cell, the grid cell CF is 100%. Yet with higher CF, autoconversion decreases. In the microphysics scheme, the rate of change of cloud liquid due to autoconversion is proportional to $CF \times (LCC/CF)^{7/3}$ or, in a frequently invoked limiter, $\ln(LCC/CF) \times LCC$ (see Rotstayn 1997). In other words, if CC is more widely distributed over a higher CF, it triggers less autoconversion. So, a rise in CF, unmatched by an increase in CC (since CC is in fact more difficult to form with the RHc100 condition), causes a decrease in autoconversion leading to a cycle slowdown as expected. This result highlights both the noninterchangeability of CC and CF as cloud tracers and the importance of considering the details of a microphysics scheme when evaluating the usefulness of performing drastic alterations.

The bigger picture highlighted by the RHc100 case is the significance of the storm tracks interrupting isentropic flow and the way in which details of the macrophysics scheme can thus have such significant effects. (Accounting for such phenomena is lacking in advection–condensation theory.) Here,

sub-grid-scale RH has a significant effect on extratropical clouds by affecting the storm track locations and altering the frequency of high-RH values. Relocated storm tracks could also have significant effects on shortwave radiation not explored here, contributing to the usefulness of RH_c as a tuning parameter for radiative balance. A potential emergent constraint on storm track response [which varies significantly in GCMs, as noted in Bender et al. (2012)] could inform RH_c choice. Thus, the RHc100 case also emphasizes the additional nonradiative impacts of tuning through RH_c, particularly on redistributing WV and precipitation.

c. Sedimentation perturbation: noRESS

As described previously, one of the most noteworthy differences between saturation adjustment and a full cloud scheme is the addition of two significant sources of WV: rain evaporation and snow sublimation (RESS). As seen in Fig. 1, column-integrated RESS have a significant presence at all latitudes, providing an even stronger source of WV than surface evaporation poleward of approximately 50°. Figure 2b shows that together they contribute approximately 17% to STET WV sources. RESS define SE as shown in Fig. 3 with one-fifth of formed precipitation lost to RESS. Figure 6a depicts the changes in WV tendencies when RESS are no longer present in the Cloud scheme. While surface evaporation increases, the elimination of RESS yields a net decrease in WV sources (Fig. 2d). Matching this decrease, a reduction in LS condensation/deposition (WV sinks) is spatially correlated both latitudinally and vertically with the eliminated RESS (Fig. 6b). Thus, as in the RHc100 case, WV and CC cycling is weakened: the total WV/CC sources or sinks in noRESS are 13%–16% less than in the Cloud case, while still greater than in the Base case (see Fig. 2). However, at the same time, the residence time of a water molecule in the atmosphere is decreased by 7% due to the elimination of RESS as WV sources that come from recycled hydrometeors.

Without RESS as sinks of precipitation, STET precipitation increases by ~5% (8% globally) as seen in Fig. 6c and Table 2. By definition, without RESS, SE is 100%. As FE is nearly unchanged, PE increases drastically from 78.3% to 97.9% with a moderate increase in precipitation. The elimination of snow sublimation corresponds strongly with the pattern and magnitude of a decrease in ice settling, yielding only a slight change in precipitation poleward of 45°. However, in the subtropics, the elimination of rain evaporation is unmatched by decreases in autoconversion and accretion, so the precipitation increase is mostly subtropical, while the storm tracks are virtually unaffected.

This feature can be rationalized by considering the location of WV sources and sinks and the connection between these budgetary terms and the steady-state fields. From a steady-state perspective, the role of RESS in redistributing WV and moistening the atmosphere can be seen in Fig. 6d. Turning off RESS results in a significant decrease in RH (up to 6%), especially in the subtropics and the polar lower troposphere. Additional experiments were performed with RESS turned off locally, including only
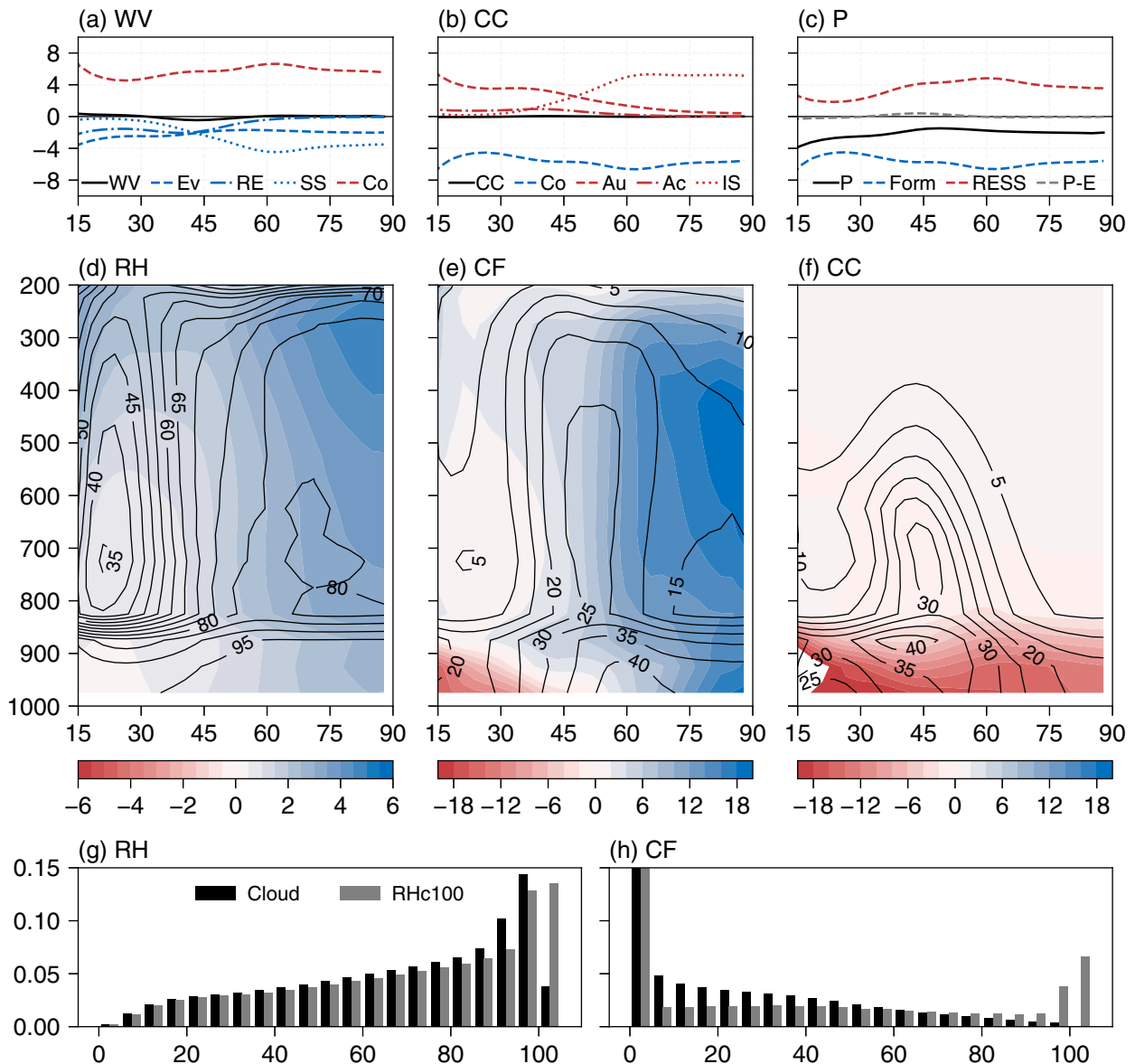
FIG. 5. Key variable changes in RHc100 perturbation from Cloud control: absolute differences in zonally averaged (a) WV, (b) CC, and (c) P tendency terms (10^{-6} kg m^{-2} s^{-1}); absolute differences in (d) RH, (e) CF, and (f) CC as shading with Cloud case values as contours (5%, 5%, and 5×10^{-6} kg kg^{-1} spacing, respectively); comparison of normalized histograms of (g) RH and (h) CF in Cloud (black) and RHc100 (gray) cases from daily data (x-axis units of percent) between 15° and 90° and 850 and 250 hPa, with the y axis cut off at 0.15. For (a)–(c), the WV, CC, and P tendency difference terms that are shown are as defined in Fig. 1 (10^{-6} kg m^{-2} s^{-1}), where a positive tendency difference denotes an increase in a WV/CC/P-increasing process or a decrease in a WV/CC/P-decreasing process. For (a)–(f), variables have been zonally averaged and the x axis is latitude; for (d)–(f), the y axis is pressure (hPa). For (g)–(h), histogram bins have widths of 5% and are all half-open except for the last bin: [0, 5), [5, 10), ..., [100, 105].

between 15° and 45° or elsewhere (not shown). These runs resulted in RH being only reduced (with any significance) in the regions where RESS is turned off, demonstrating the local nature of the contribution of RESS to moisture. In redistributing WV, RESS also play a significant role in the cloud distribution. Without RESS, both CF and CC decrease globally as shown in Figs. 6e and 6f. The change in CF is of a similar pattern to the change in RH in the polar extratropics, while the change in CC is more concentrated in the storm tracks (where CC is larger to begin

with). RH and CF changes are directly connected, as confirmed by considering histograms of extratropical RH and CF (Figs. 6g,h). The noRESS case shifts occurrences of RH away from higher values (>95%) in the extratropical free troposphere corresponding with a decrease in CF concentrated where RH values are highest to begin with.

The connection between budgetary and steady-state changes is nuanced. Globally, the general reduction in RH is to be expected since the lack of RESS results in a drying of the boundary layer.
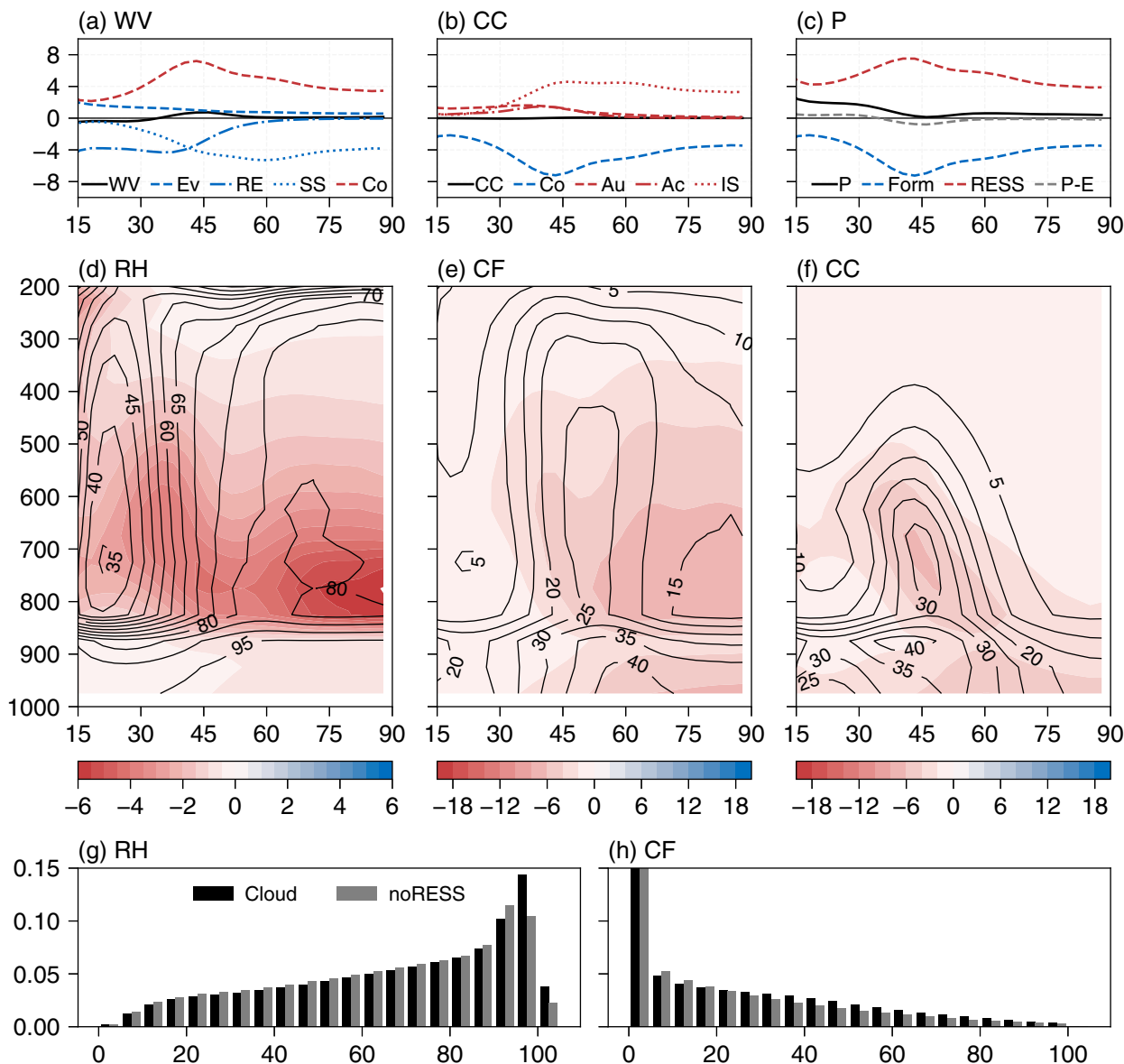
FIG. 6. As Fig. 5, but for noRESS perturbation.

This drying triggers more surface evaporation, but no other sources of WV. Decreased higher values of RH lead to decreased clouds. But, spatially, the areas of largest RH change (free troposphere, especially the polar extratropics) do not coincide with the locations of largest RESS tendency. RESS together provide a significant source of WV throughout the boundary layer and free troposphere, especially in the tropics (not shown). However, while RESS are smallest in the extratropics, its relative importance as a source of WV is greatest there (see Fig. 1a). While surface evaporation can easily increase below 850 hPa to replace RESS as a source of WV in the boundary layer (which is always nearly saturated), its ability to replenish moisture above 850 hPa depends on circulation. The rising motions induced by the Hadley circulation in the tropics allow humidity (and thus

clouds) to be less affected by the loss of RESS. In contrast, in the polar regions where less vertical motion takes place and horizontal transport is more important for WV, the lower troposphere above 850 hPa experiences significant drying.

Thus, in the storm tracks and high latitudes, the increase in precipitation is small since the elimination of RESS dries the region creating two opposing effects. Precipitation is increased since SE is now 100%, but this increase is nearly balanced by a reduction in precipitation due to less moisture and thus fewer precipitating clouds in the region. However, in the subtropics and midlatitudes, the direct increase in precipitation is largely unbalanced since clouds are less affected (as clouds are few to begin with so humidity decreases have little effect). This local role of RESS is further seen in the fact that $P - E$ (Fig. 6c)
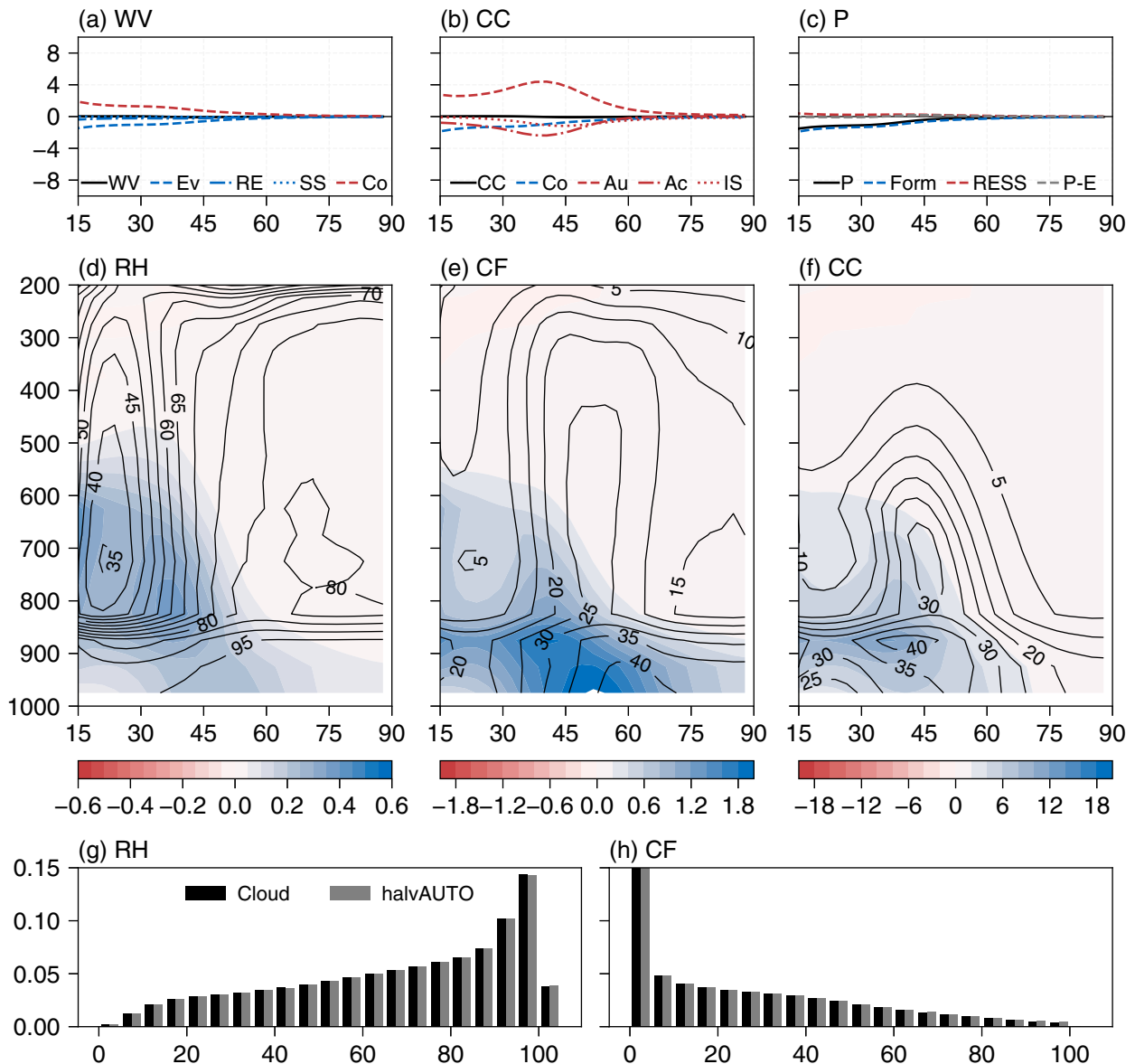
FIG. 7. As Fig. 5, but for halvAUTO perturbation, except that the color-bar scale is reduced by a factor of 10 for (d) and (e).

remains largely unchanged. Ultimately, the role of RESS in the free troposphere is to increase RH (and ultimately clouds) by providing an additional source of WV, while decreasing precipitation and—to a much greater extent—the PE through the introduction of an atmospheric sink for hydrometeors.

d. Formation perturbation: halvAUTO

In the halvAUTO case, autoconversion decreases in the STET region by 29%. Accretion and ice settling increase by 19% and 4%, respectively, to keep total STET CC sinks only 3% less than in the Cloud case. This rebalancing can be conceptualized as weakened autoconversion causing more cloud liquid to be present to be scavenged by ice through accretion and subsequently settling. Similarly, in the doubAUTO case, STET

autoconversion increases by 34%, accretion decreases by 22%, and ice settling increases by 6%, such that total CC sinks are only 3% more than in the Cloud case. These changes can be seen in Figs. 2e and 2f. In both cases the relative balance of the WV sources and sinks is roughly unchanged. Noting the parallel opposing changes in halvAUTO and doubAUTO, we focus primarily on halvAUTO.

Figure 7a shows that latitudinally the WV balance is unchanged with decreases in LS condensation, surface evaporation, and rain evaporation balancing each other. Similarly, the CC balance (Fig. 7b) stays latitudinally unchanged with a decrease in LS condensation balanced by the net decreases in CC sinks. The opposing changes in autoconversion and accretion are similar in their spatial pattern, but the decrease in autoconversion is stronger,

resulting in less precipitation as shown in Fig. 7c. These changes are principally equatorward of 60° since that is where autoconversion is most significant in the first place (Fig. 1b).

Across the STET region, precipitation decreases in the halvAUTO case by 3% and increases in the doubAUTO case by 4%, similar to how the strength of the WV/CC cycle changes. From an efficiency perspective (see Table 2), CE and FE change slightly in the same direction as changes in precipitation, decreasing in halvAUTO in line with a cycle slowdown. SE also changes slightly but in the opposite way: with decreased net formation but a proportionally larger decrease in RESS in the halvAUTO case, SE increases slightly. The FE and SE effects balance such that PE is minimally affected. This finding holds true for smaller and larger alterations to autoconversion, accretion, and N except when an artificial decrease in a process is so large that the other processes cannot keep the WV/CC cycle roughly constant. For example, when autoconversion is completely eliminated, total STET CC sinks decrease by 6% as accretion cannot come close to making up for the difference reducing FE to 90.4% and PE to 72.1%. However, apart from such limiting cases, changes in budgetary terms and efficiencies are roughly linear. The residence time increases with halvAUTO with weakened precipitation since a water molecule now spends a longer time in the atmosphere as CC before precipitating, while the doubAUTO case shows a corresponding decrease in residence time.

From a steady-state perspective, in the halvAUTO case, RH, CF, and CC all increase as shown in Figs. 7d–f. The significant changes are spatially similar, concentrated equatorward of 60° (where the net decrease in CC sinks was strongest) and below ~500 hPa, peaking in the storm tracks. These steady-state changes described are qualitatively opposite in the doubAUTO case (not shown). Of note, the steady-state RH and cloud fields change not in response to a shift in the balance between autoconversion and accretion, but in response to changes in total sources/sinks. When WV/CC cycling strengthened due to increased autoconversion, increased accretion, or decreased N, a reduction of RH, CF, and CC resulted. Opposite changes are associated with WV/CC cycling weakening. Rebalancing autoconversion and accretion must have a relatively innocuous effect on RH and clouds in and of itself.

Why does a weakened (strengthened) cycle increase (decrease) RH and clouds? It is important to note that this generalization does not extend past these perturbations. (The pattern is followed in the RHc100 case discussed previously but not in the noRESS case, possibly because of the significant spatial and physical differences resulting from replacing RESS as WV sources with enhanced surface evaporation.) However, in the absence of other changes (such as adding sources and sinks from the Base to the Cloud case), a longer (shorter) residence time for a water molecule in the atmosphere could be expected to correspond to an increase (decrease) in the steady-state fields that represent the forms that a water molecule takes as it resides in the atmosphere. Additionally, steady-state RH is directly connected to the WV cycle through surface evaporation since it is formulated as a function of subsaturation. RH is connected to CF as demonstrated by considering histograms of RH and CF (Figs. 7g,h):

the halvAUTO case slightly shifts occurrences of RH toward the highest values (>100%). Without any significant changes to the cloud physics beyond a rebalancing of autoconversion and accretion, CC can logically be expected to follow CF.

Thus, the formation perturbations demonstrate the resilience of this cloud microphysics scheme to changes in the balance of formation tendencies in terms of PE. Additionally, the general patterns for steady-state consequences of the WV/CC cycle weakening or strengthening emerge, showing how steady-state fields are affected by changes in residence time. A weakened cycle, apart from other changes in cloud physics, leads to an increased residence time and increased steady-state RH, CC, and CF. Conversely, a strengthened cycle, apart from other changes in cloud physics, leads to a decreased residence time and decreased steady-state RH, CC, and CF.

4. Discussion and conclusions

a. Summary

The general picture that emerges from this idealized modeling study is that circulation sets the basic pattern of moisture and precipitation, as seen through the first-order similarity between the two control cases. In the perturbation runs, details of the physics of condensation and sedimentation also have substantial effects on humidity, clouds, and precipitation. However, it is noteworthy that while RH does differ substantially (in certain extratropical regions) between the control cases, precipitation does not, as the precipitation changes in the condensation and sedimentation perturbations (RHc100 and noRESS) are of opposing sign. A secondary picture is the utility of this idealized GCM for understanding physical controls of free tropospheric clouds and responses to perturbations since key processes can be cleanly isolated. The saturation adjustment scheme (Base case) shows gross RH features, as expected from advection–condensation theory, but cloud processes refine the features. In particular, cloud macrophysics are important since thresholds for cloud formation change cloud distribution (including the CF/CC ratio) and hence high RH and storm track location due to isentropic transport of moisture as shown in the RHc100 run. Cloud microphysics are equally important, adding a key component through the re-evaporation of hydrometeors (RESS) changing RH values by a similar magnitude, as much as 5%–6%. However, the formation perturbations demonstrate that the balance of precipitation-forming processes (here autoconversion and accretion) have little significance for RH, cloudiness, precipitation, and especially PE.

b. Advection–condensation theory

As was discussed previously, there are, on the surface, three differences between a saturation adjustment scheme (or advection–condensation theory) and a full cloud scheme: RH_c, RESS, and the presence of CC, which can be advected and/or subject to LS evaporation/sublimation. The first two differences are here individually directly removed, but the third must be explored as a residual in the RHc100_noRESS experiment where we remove the RH_c and RESS effects together from the Cloud case. If these three identified differences are exhaustive, RHc100_noRESS represents the effect of adding
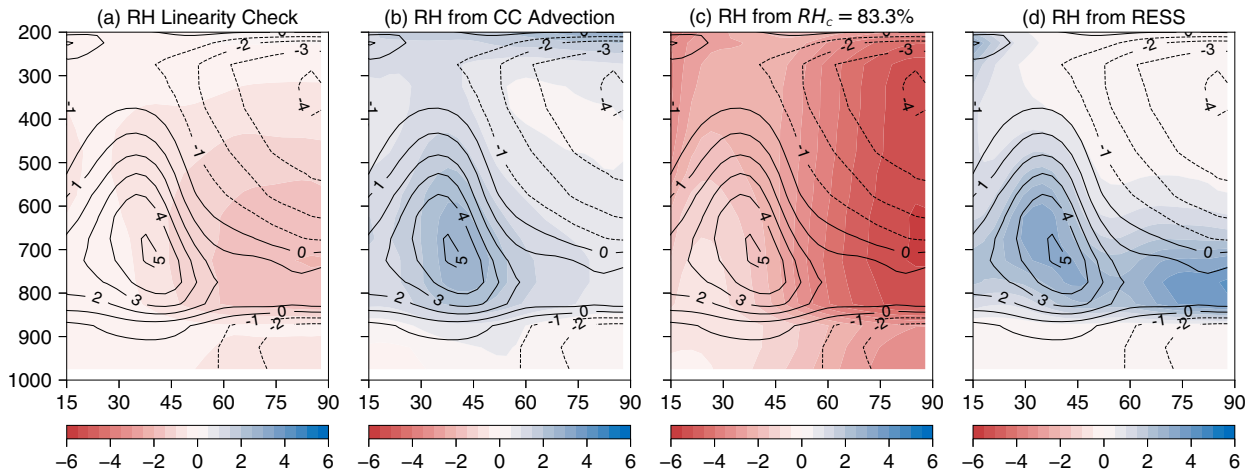
FIG. 8. Comparison of absolute RH differences (%) between control cases and intermediate setups: (a) RHc100 plus noRESS minus RHc100_noRESS minus Cloud (linearity check: should be 0 if $RH_c = 83.3\%$ and RESS effects sum linearly), (b) RHc100_noRESS minus Base (CC advection effect) as shading, (c) noRESS minus RHc100_noRESS ($RH_c = 83.3\%$ effect) as shading, and (d) RHc100 minus RHc100_noRESS (RESS effect) as color shading. All contours are Cloud minus Base difference with a spacing of 1%. Variables have been zonally averaged, and the x and y axes are latitude and pressure (hPa), respectively.

CC to the Base case. Additionally, if the RH_c and RESS effects are linearly additive, we can mathematically manipulate the various experiments to isolate the separate effects of RH_c and RESS added to the Base case (as opposed to removing these effects from the Cloud case as was described in section 3). To this end, Fig. 8 explores to what extent the RH_c and RESS effects are linearly additive, to what extent they can explain the full difference between the Base and Cloud controls, and the characteristics of the residual differences that can be attributed to CC advection.

The RHc100 run includes RESS and advection effects, the noRESS run includes RHc and advection effects, and the RHc100_noRESS run is just the advection effect. So, we can test for linearity of the RH_c and RESS effects by comparing RHc100 plus noRESS minus RHc100_noRESS (Fig. 8a). The combination appears to be mostly linear except in the free tropospheric high latitudes where both RHc100 and noRESS runs had significant, but opposing, effects. RHc100 leads to moistening and noRESS to drying; linear addition overemphasizes drying or underemphasizes moistening. A possible mechanism is that when both are implemented, there is less moisture (from noRESS) to be exported to the high latitudes (in RHc100), but this effect should be minimal as noRESS minimally dries the boundary layer. A more likely explanation is that since in RHc100, RESS together decrease by over 50%, the noRESS drying effect is dampened when combined. But since they combine nearly linearly, we can separately analyze the three effects of adding a cloud scheme to a saturation adjustment scheme.

When adding a cloud scheme to a saturation adjustment scheme, advection and LS evaporation/sublimation [and any other residual effects: for example, nucleation barrier and incomplete fallout in cirrus as noted by Liu et al. (2010)] moisten the free tropospheric subtropics and midlatitudes (Fig. 8b) as well as

the polar stratosphere. Implementing an RH_c of 83.3% dries the high latitudes (Fig. 8c) by allowing for more condensation and precipitation of moisture before it is isentropically transported to the poles. RESS moisten the free troposphere, most strongly in the storm tracks and lower polar regions (Fig. 8d), by adding an additional source of WV above the boundary layer.

Thus, this work highlights the key deficiencies with an advection–condensation paradigm. The relatively small residual effects seen when comparing RHc100_noRESS minus Base with Cloud minus Base (Fig. 8b) suggest that RH_c and RESS are the key ways in which a cloud scheme alters the RH distribution from advection–condensation theory alone, in the absence of cloud processes altering the circulation through latent heat release or cloud radiative effects. The RESS effect is a cloud microphysical effect already noted as missing from the advection–condensation paradigm and important to moistening the subtropics. Here, however, we also highlight its importance for moistening the polar regions where less vertical motion makes surface evaporation less effective at moistening the free troposphere. In contrast, RH_c is a macrophysical effect, an artifact of parameterizations attempting to represent the RH variability present in the real world. Here we emphasize the importance of considering sub-grid-scale humidity distribution to allow clouds to form in appropriate latitudinal locations (a problem that increased resolution alone may not fix). As Sherwood et al. (2010) noted, these components of why the advection–condensation paradigm is inadequate are critical to understand so as to accurately model not just climatological values, but importantly changes in RH (and hence clouds and precipitation) with warming.

c. Outlook

The picture presented here is likely to change significantly with warming. While the advection–condensation paradigm

suggests that free tropospheric RH is unlikely to change significantly with uniform warming (Sherwood et al. 2010), the specific deficiencies of advection–condensation theory explored here confound predicting changes in RH with warming, already complicated by nonuniform warming. Any changes in RH could also have implications for $P - E$ changes, because the wet-get-wetter paradigm (Held and Soden 2006) is predicated on unchanged lower-tropospheric RH and flow. Sherwood et al. (2014) identified a mixing-induced low cloud feedback where enhanced mixing with warming dehydrates the boundary layer. Here, as in advection–condensation theory, we highlighted the connection between subtropical boundary layer humidity and polar upper tropospheric humidity because of eddy isentropic transport. In addition to the complications of dynamical effects, because of the Clausius–Clapeyron relation, WV transport is expected to increase with warming for thermodynamic reasons (Lavers et al. 2015). And as noted in the introduction, replacement of ice with liquid in mixed-phase clouds with warming may also affect moisture and cloud distribution through changes in precipitation efficiency. Thus, modeling the mechanisms controlling extratropical humidity and clouds accurately is critical for confidently forecasting future change.

Our perturbation results demonstrate the significance of key processes for defining steady-state patterns of humidity and cloudiness, implying a strong need to constrain processes such as RESS and sub-grid-scale RH to ensure the physical grounding of parameterizations so that responses to altered forcings will also be physical. For example, in using RH_c as a GCM tuning parameter, the multiple ways in which it effects radiative balance—such as through shifted storm track cloud maxima and opposing changes in CF and CC—should be carefully considered, especially as they may be obscured or amplified by dynamical effects. In addition, although accr/auto (or N) was not important here in terms of affecting steady-state fields or average precipitation, it is likely to have other effects as discussed in the introduction, including modulating the intensity of precipitation events. Our results suggest that the strength of warm rain processes as a whole (accretion + autoconversion) plays a role in defining RH, clouds, and precipitation distribution and thus is an important parameter to constrain, not just accr/auto. By separately analyzing the effects on CF and CC and their connection to changes in RH and various components of the water cycle, this study highlighted the need to carefully dissect the physical mechanisms for change instead of relying on generalizations. For example, as demonstrated in the RHc100 perturbation, cloud response cannot be directly predicted from changes in average RH. Relationships among RH, CF, and CC in a cloud scheme may be non-intuitive and are certainly nontrivial. CC and CF have varying levels of importance for cloud radiative effects depending on regime and saturation, so individual local effects are consequential.

Comparing the significance of various controls of clouds cannot be precise in this idealized, decoupled framework. Nor does this study explore the relative significance of various cloud feedbacks to anthropogenic forcings. Yet, by allowing for a detailed exploration of cloud physics decoupled from circulation, this type of idealized model could play a key role in

the model hierarchy for reducing uncertainty surrounding cloud feedback. In comprehensive GCMs with coupled feedbacks, circulation feedbacks (particularly shifts in the extratropical jets) have been demonstrated to be less significant than thermodynamic mechanisms of mixed-phase clouds in creating the shortwave extratropical cloud feedback (Wall and Hartmann 2015; Ceppi and Hartmann 2016). This finding suggests that cloud parameterization mechanisms relating to mixed-phase clouds may play a significant role in constraining extratropical cloudiness, an area explored in related work with the idealized setup used in this paper (Frazer and Ming 2022).

In summary, this study takes a step forward in elucidating physical mechanisms controlling extratropical clouds while highlighting the importance of identifying and adequately representing these mechanisms so as to accurately simulate the cloud feedbacks associated with climate change.

Data availability statement. The output from the simulations described in this paper is archived at the Geophysical Fluid Dynamics Laboratory and is available upon request.

REFERENCES

Bender, F. A. M., V. Ramanathan, and G. Tselioudis, 2012: Changes in extratropical storm track cloudiness 1983–2008: Observational support for a poleward shift. *Climate Dyn.*, **38**, 2037–2053, https://doi.org/10.1007/s00382-011-1065-6.

Bony, S., and Coauthors, 2015: Clouds, circulation and climate sensitivity. *Nat. Geosci.*, **8**, 261–268, https://doi.org/10.1038/ngeo2398.

Ceppi, P., and D. L. Hartmann, 2016: Clouds and the atmospheric circulation response to warming. *J. Climate*, **29**, 783–799, https://doi.org/10.1175/JCLI-D-15-0394.1.

——, ——, and M. J. Webb, 2016: Mechanisms of the negative shortwave cloud feedback in middle to high latitudes. *J. Climate*, **29**, 139–157, https://doi.org/10.1175/JCLI-D-15-0327.1.

——, F. Brient, M. D. Zelinka, and D. L. Hartmann, 2017: Cloud feedback mechanisms and their representation in global climate models. *Wiley Interdiscip. Rev. Climate Change*, **8**, e465, https://doi.org/10.1002/wcc.465.

Frazer, M. E., and Y. Ming, 2022: Understanding the extratropical liquid water path feedback in mixed-phase clouds with an idealized global climate model. *J. Climate*, **35**, 2391–2406, https://doi.org/10.1175/JCLI-D-21-0334.1.

Frierson, D. M. W., I. M. Held, and P. Zurita-Gotor, 2006: A gray-radiation aquaplanet moist GCM. Part I: Static stability and eddy scale. *J. Atmos. Sci.*, **63**, 2548–2566, https://doi.org/10.1175/JAS3753.1.

Galewsky, J., A. Sobel, and I. M. Held, 2005: Diagnosis of subtropical humidity dynamics using tracers of last saturation. *J. Atmos. Sci.*, **62**, 3353–3367, https://doi.org/10.1175/JAS3533.1.

Geoffroy, O., S. C. Sherwood, and D. Fuchs, 2017: On the role of the stratiform cloud scheme in the inter-model spread of cloud feedback. *J. Adv. Model. Earth Syst.*, **9**, 423–437, https://doi.org/10.1002/2016MS000846.

Gettelman, A., H. Morrison, C. R. Terai, and R. Wood, 2013: Microphysical process rates and global aerosol–cloud interactions. *Atmos. Chem. Phys.*, **13**, 9855–9867, https://doi.org/10.5194/acp-13-9855-2013.

——, ——, ——, and ——, 2014: Corrigendum to "Microphysical process rates and global aerosol–cloud interactions." *Atmos. Chem. Phys.*, **14**, 9099–9103, https://doi.org/10.5194/acp-14-9099-2014.

Held, I. M., 2005: The gap between simulation and understanding in climate modeling. *Bull. Amer. Meteor. Soc.*, **86**, 1609–1614, https://doi.org/10.1175/BAMS-86-11-1609.

——, 2014: Simplicity amid complexity. *Science*, **343**, 1206–1207, https://doi.org/10.1126/science.1248447.

——, and M. J. Suarez, 1994: A proposal for the intercomparison of the dynamical cores of atmospheric general circulation models. *Bull. Amer. Meteor. Soc.*, **75**, 1825–1830, https://doi.org/10.1175/1520-0477(1994)075<1825:APFTIO>2.0.CO;2.

——, and T. Schneider, 1999: The surface branch of the zonally averaged mass transport circulation in the troposphere. *J. Atmos. Sci.*, **56**, 1688–1697, https://doi.org/10.1175/1520-0469(1999)056<1688:TSBOTZ>2.0.CO;2.

——, and B. J. Soden, 2006: Robust responses of the hydrological cycle to global warming. *J. Climate*, **19**, 5686–5699, https://doi.org/10.1175/JCLI3990.1.

Jeevanjee, N., P. Hassanzadeh, S. Hill, and A. Sheshadri, 2017: A perspective on climate model hierarchies. *J. Adv. Model. Earth Syst.*, **9**, 1760–1771, https://doi.org/10.1002/2017MS001038.

Jiang, H., G. Feingold, and A. Sorooshian, 2010: Effect of aerosol on the susceptibility and efficiency of precipitation in warm trade cumulus clouds. *J. Atmos. Sci.*, **67**, 3525–3540, https://doi.org/10.1175/2010JAS3484.1.

Jing, X., K. Suzuki, H. Guo, D. Goto, T. Ogura, T. Koshiro, and J. Mülmenstädt, 2017: A multimodel study on warm precipitation biases in global models compared to satellite observations. *J. Geophys. Res. Atmos.*, **122**, 11 806–11 824, https://doi.org/10.1002/2017JD027310.

Kelly, K., A. Tuck, and T. Davies, 1991: Wintertime asymmetry of upper tropospheric water between the Northern and Southern Hemispheres. *Nature*, **353**, 244–247, https://doi.org/10.1038/353244a0.

Klein, S. A., and Coauthors, 2009: Intercomparison of model simulations of mixed-phase clouds observed during the ARM Mixed-Phase Arctic Cloud Experiment. I: Single-layer cloud. *Quart. J. Roy. Meteor. Soc.*, **135**, 979–1002, https://doi.org/10.1002/qj.416.

Laliberté, F., T. Shaw, and O. Pauluis, 2012: Moist recirculation and water vapor transport on dry isentropes. *J. Atmos. Sci.*, **69**, 875–890, https://doi.org/10.1175/JAS-D-11-0124.1.

Langhans, W., K. Yeo, and D. M. Romps, 2015: Lagrangian investigation of the precipitation efficiency of convective clouds. *J. Atmos. Sci.*, **72**, 1045–1062, https://doi.org/10.1175/JAS-D-14-0159.1.

Lavers, D. A., F. M. Ralph, D. E. Waliser, A. Gershunov, and M. D. Dettinger, 2015: Climate change intensification of horizontal water vapor transport in CMIP5. *Geophys. Res. Lett.*, **42**, 5617–5625, https://doi.org/10.1002/2015GL064672.

Liu, Y. S., S. Fueglistaler, and P. H. Haynes, 2010: Advection–condensation paradigm for stratospheric water vapor.

J. Geophys. Res., **115**, D24307, https://doi.org/10.1029/2010JD014352.

McCoy, D. T., D. L. Hartmann, M. D. Zelinka, P. Ceppi, and D. P. Grosvenor, 2015: Mixed-phase cloud physics and Southern Ocean cloud feedback in climate models. *J. Geophys. Res. Atmos.*, **120**, 9539–9554, https://doi.org/10.1002/2015JD023603.

——, I. Tan, D. L. Hartmann, M. D. Zelinka, and T. Storelvmo, 2016: On the relationships among cloud cover, mixed-phase partitioning, and planetary albedo in GCMs. *J. Adv. Model. Earth Syst.*, **8**, 650–668, https://doi.org/10.1002/2015MS000589.

——, D. L. Hartmann, and M. D. Zelinka, 2018: Mixed-phase cloud feedbacks. *Mixed-Phase Clouds: Observations and Modeling*, C. Andronache, Ed., Elsevier, 215–236, https://doi.org/10.1016/B978-0-12-810549-8.00009-X.

Michibata, T., and T. Takemura, 2015: Evaluation of autoconversion schemes in a single model framework with satellite observations. *J. Geophys. Res. Atmos.*, **120**, 9570–9590, https://doi.org/10.1002/2015JD023818.

Ming, Y., and I. M. Held, 2018: Modeling water vapor and clouds as passive tracers in an idealized GCM. *J. Climate*, **31**, 775–786, https://doi.org/10.1175/JCLI-D-16-0812.1.

Pierrehumbert, R. T., 1998: Lateral mixing as a source of subtropical water vapor. *Geophys. Res. Lett.*, **25**, 151–154, https://doi.org/10.1029/97GL03563.

——, H. Brogniez, and R. Roca, 2007: On the relative humidity of the atmosphere. *The Global Circulation of the Atmosphere*, T. Schneider and A. H. Sobel, Eds., Princeton University Press, 143–185.

Quaas, J., and Coauthors, 2009: Aerosol indirect effects—General circulation model intercomparison and evaluation with satellite data. *Atmos. Chem. Phys.*, **9**, 8697–8717, https://doi.org/10.5194/acp-9-8697-2009.

——, and Coauthors, 2020: Constraining the Twomey effect from satellite observations: Issues and perspectives. *Atmos. Chem. Phys.*, **20**, 15 079–15 099, https://doi.org/10.5194/acp-20-15079-2020.

Rotstayn, L. D., 1997: A physically based scheme for the treatment of stratiform clouds and precipitation in large-scale models. I: Description and evaluation of the microphysical processes. *Quart. J. Roy. Meteor. Soc.*, **123**, 1227–1282, https://doi.org/10.1002/qj.49712354106.

——, B. F. Ryan, and J. J. Katzfey, 2000: A scheme for calculation of the liquid fraction in mixed-phase clouds in large-scale models. *Mon. Wea. Rev.*, **128**, 1070–1088, https://doi.org/10.1175/1520-0493(2000)128<1070:ASFCOT>2.0.CO;2.

Shepherd, T. G., 2014: Atmospheric circulation as a source of uncertainty in climate change projections. *Nat. Geosci.*, **7**, 703–708, https://doi.org/10.1038/ngeo2253.

Sherwood, S. C., R. Roca, T. M. Weckwerth, and N. G. Andronova, 2010: Tropospheric water vapor, convection, and climate. *Rev. Geophys.*, **48**, RG2001, https://doi.org/10.1029/2009RG000301.

——, S. Bony, and J.-L. Dufresne, 2014: Spread in model climate sensitivity traced to atmospheric convective mixing. *Nature*, **505**, 37–42, https://doi.org/10.1038/nature12829.

——, and Coauthors, 2020: An assessment of Earth's climate sensitivity using multiple lines of evidence. *Rev. Geophys.*, **58**, e2019RG000678, https://doi.org/10.1029/2019RG000678.

Stephens, G. L., 1978: Radiation profiles in extended water clouds. II. Parameterization schemes. *J. Atmos. Sci.*, **35**, 2123–2132, https://doi.org/10.1175/1520-0469(1978)035<2123:RPIEWC>2.0.CO;2.

Stevens, B., and S. Bony, 2013: What are climate models missing? *Science*, **340**, 1053–1054, https://doi.org/10.1126/science.1237554.

Sun, D.-Z., and R. S. Lindzen, 1993: Distribution of tropical tropospheric water vapors. *J. Atmos. Sci.*, **50**, 1643–1660, https://doi.org/10.1175/1520-0469(1993)050<1643:DOTTWV>2.0.CO;2.

Trenberth, K. E., 1998: Atmospheric moisture residence times and cycling: Implications for rainfall rates and climate change. *Climatic Change*, **39**, 667–694, https://doi.org/10.1023/A:1005319109110.

Wall, C. J., and D. L. Hartmann, 2015: On the influence of poleward jet shift on shortwave cloud feedback in global climate models. *J. Adv. Model. Earth Syst.*, **7**, 2044–2059, https://doi.org/10.1002/2015MS000520.

Wu, P., B. Xi, X. Dong, and Z. Zhang, 2018: Evaluation of autoconversion and accretion enhancement factors in general circulation model warm-rain parameterizations using ground-based measurements over the Azores. *Atmos. Chem. Phys.*, **18**, 17 405–17 420, https://doi.org/10.5194/acp-18-17405-2018.

Yang, H., and R. T. Pierrehumbert, 1994: Production of dry air by isentropic mixing. *J. Atmos. Sci.*, **51**, 3437–3454, https://doi.org/10.1175/1520-0469(1994)051<3437:PODABI>2.0.CO;2.

Zhao, M., 2014: An investigation of the connections among convection, clouds, and climate sensitivity in a global climate model. *J. Climate*, **27**, 1845–1862, https://doi.org/10.1175/JCLI-D-13-00145.1.

——, I. M. Held, S.-J. Lin, and G. A. Vecchi, 2009: Simulations of global hurricane climatology, interannual variability, and response to global warming using a 50-km resolution GCM. *J. Climate*, **22**, 6653–6678, https://doi.org/10.1175/2009JCLI3049.1.